A Cable-Driven Parallel Robot with Full-Circle End-Effector Rotations

Marceau Métillon, Saman Lessanibahri, Philippe Cardou, Kévin Subrin, Stéphane Caro

A CABLE-DRIVEN PARALLEL ROBOT WITH FULL-CIRCLE END-EFFECTOR ROTATIONS

Marceau Métillon[1,2], **Saman Lessanibahri**[1,5], **Philippe Cardou**[3], **Kévin Subrin**[1,4], **Stéphane Caro**[1,2]*
[1] Laboratoire des Sciences du Numérique de Nantes (LS2N), UMR CNRS 6004, 44300 Nantes, France
[2] Centre National de la Recherche Scientifique (CNRS), 44321 Nantes, France
[3] Laboratoire de robotique, Département de génie mécanique, Université Laval, Québec, QC, Canada
[4] Univérsité de Nantes, IUT, 44470 Carquefou, France
[5] École Centrale de Nantes, 44321 Nantes, France
Emails: marceau.metillon@ls2n.fr, saman.lessanibahri@ls2n.fr
pcardou@gmc.ulaval.ca, kevin.subrin@ls2n.fr, stephane.caro@ls2n.fr

ABSTRACT

Cable-Driven Parallel Robots (CDPRs) offer high payload capacities, large translational workspace and high dynamic performances. The rigid base frame of the CDPR is connected in parallel to the moving platform using cables. However, their orientation workspace is usually limited due to cable/cable and cable/moving platform collisions. This paper deals with the designing, modelling and prototyping of a hybrid robot. This robot, which is composed of a CDPR mounted in series with a Parallel Spherical Wrist (PSW), has both a large translational workspace and an unlimited orientation workspace. It should be noted that the six degrees of freedom (DOFs) motions of the moving platform of the CDPR, namely, the base of the PSW, and the three-DOFs motion of the PSW are actuated by means of eight actuators fixed to the base. As a consequence, the overall system is underactuated and its total mass and inertia in motion is reduced.

1 INTRODUCTION

A Cable Driven Parallel Robot (CDPR) belongs to a particular class of parallel robots where a moving platform is linked to a base frame using cables. Motors are mounted on a rigid base frame and drive winches. Cable coiled on these winches are routed through exit points located on the rigid frame to anchor points on the moving platform. The pose (position and orientation) of the moving platform is determined by controlling the cable lengths.

CDPRs have several advantages compared to classical parallel robots. They are inexpensive and can cover large workspaces [1]. The lightweight cables contribute to the lower inertia of the moving platform and consequently to a better dynamic performance over classical parallel robots [2]. Another characteristic of the CDPRs is their reconfigurability. Changing the overall geometry of the robot can be done by changing the exit points and anchor points.

Reconfigurability of the CDPRs is suitable for versatile applications especially in an industrial context [3, 4, 5]. CDPRs have drawn researchers' interests towards robotic applications such as pick-and-place operations, robotic machining, manipulation, intralogistics measurements and calibration systems [6].

CDPRs can offer an extremely large three-degrees of freedom translational workspace, but their orientation workspace is usually limited due to cable/cable and cable/moving platform collisions. Cable interferences can be divided into cable-cable and cable-environment interferences [7]. For a given pose of the moving platform, cable-cable collision may occur by changing the moving platform orientation. Cable-environment collisions refer to the interferences between the moving platform and its surrounding environment.

This paper presents the concept of a hybrid manipulator with decoupled translation and orientation motions of the moving platform. It is called hybrid since two parallel mechanisms

*Address all correspondence to this author.

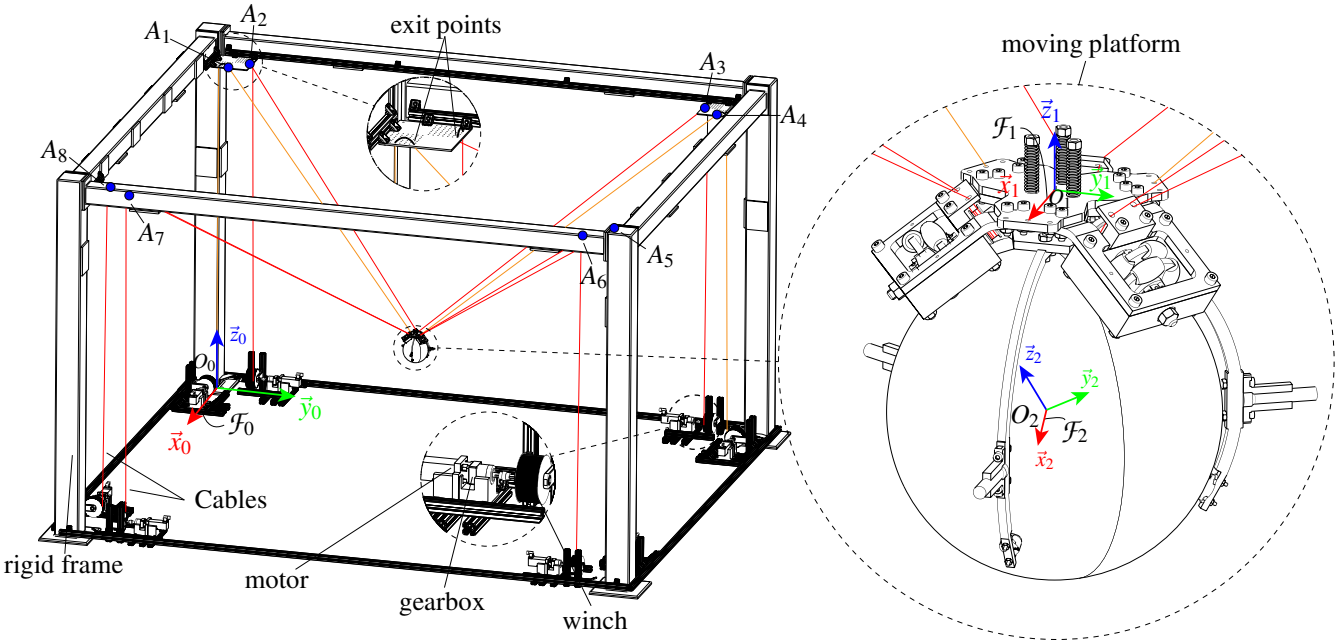

Figure 1: CDPR with full-circle end effector rotations

are connected in series, namely, a CDPR and a parallel spherical wrist [8]. In [9], a bi-actuated cable is used in order to improve the orientation capacity of the end-effector.

In [10] a hybrid CDPR uses a cable-loop for remote actuation of an embedded hoist mechanism on the moving platform. In [11] a moving platform embedding a two-DOFs differential gear set mechanism is presented allowing the two-DOFs unlimited rotational motions of the end-effector. Thanks to cable-loops (bi-actuated cables), the embedded mechanisms are actuated by transmitting power through cables from motors, which are fixed on the ground, to the moving platform. Therefore, by remote actuation through cable-loops, the tethering of the power cable to the moving platform is eliminated [12]. Moreover, a lower mass and a lower inertia of the moving platform are obtained due to the remote actuators.

In this paper the mechanical design of the manipulator under study is presented in Section 2. Its kineto-static model is described in Section 3. The static workspace of the manipulator is studied in Section 4. The methodology followed to determine the optimal cable arrangement of the system is explained in Section 5. The developed prototype of the mechanism at hand and some experimental results are shown in Section 6. Conclusions and future work are drawn in Section 7.

2 DESCRIPTION AND PARAMETRIZATION OF THE MANIPULATOR

The kinematic architecture of the manipulator consists of two parallel manipulators mounted in series. A CDPR grants a large translation workspace and a Parallel Spherical Wrist (PSW) grants an unlimited orientation workspace. This hybrid manipulator is able to combine advantages of both mechanisms in terms of large translation and orientation workspaces.

2.1 OVERALL ARCHITECTURE

Figure 1 shows the overall architecture of the manipulator with its main components, namely, winches, exit-points and the moving platform. The winches control the cable lengths, which move and actuate the moving platform. Cables are routed through exit-points located on the rigid frame and connected to anchor-points located on the moving platform.

Figure 2 shows the moving platform, which hosts a top plate assembly and embeds the PSW. The end-effector of the wrist is a sphere actuated by three cable-loops, which transmit the required power from motors fixed on the ground to the end-effector of the moving platform, namely the sphere.

The PSW is described in detail in Sec. 2.2 while the cable-loop system is presented in Sec. 2.3. The top plate has the six-DOFs and the PSW grants a large orientation workspace to the sphere providing an overall nine-DOFs workspace to the spherical end-effector regarding the base frame $\mathcal{F}_0$.

2.2 THREE-DOFs PARALLEL SPHERICAL WRIST

The concept of the PSW relies on the Atlas platform principle [13]. An end-effector is linked to the base of the wrist using a spherical joint. Three omni-wheels are linked to the wrist base with revolute joints. The end-effector is a sphere actuated by the

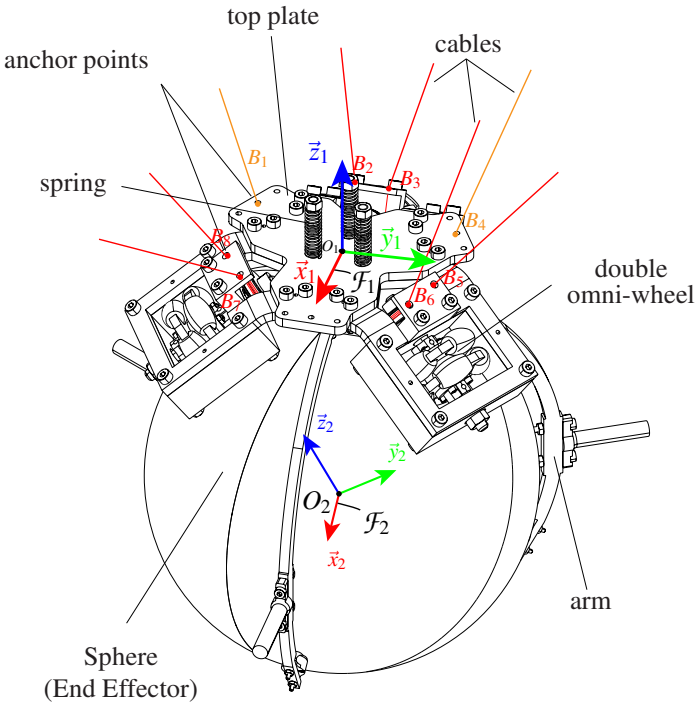

Figure 2: The moving platform

rotation of the omni-wheels. The position of the wheel relative to the sphere surface was defined to allows a singular-free and unlimited orientation of the sphere around the global $\vec{x}_0$, $\vec{y}_0$ and $\vec{z}_0$ axes as discussed in [14].

Here, the top plate of the CDPR amounts to the wrist base. Three carriage sub-assemblies are rigidly attached to the top plate. Every carriage hosts an omni-wheel. A three rigid arm platform hosts the sphere using three caster balls. Three anti-backlash compression springs are mounted on threaded rods using nuts, thus ensuring the connection of the arm platform to the top plate. The springs ensure an adjustable contact force of the omni-wheels on the sphere. The omni-wheels transmit torque to the sphere thanks to friction. Each omni-wheel is independently driven by a cable-loop system.

2.3 CABLE-LOOP PRINCIPLE

Figure 3 represents a simplified form of the cable-loop system. The latter consists of a single cable of which both ends are actuated by two motors while passing through exit-points, namely, A_1, A_2, and anchor-points, namely, B_1, B_2. The cable-loop is coiled up around a drum on the moving platform. The cable-loop drum then acquires one rotational DOFs with respect to the moving platform used to actuate a tool or to control additional degrees of freedom such as rotations over wide ranges. The purpose of the cable-loop is double. Firstly, its aim is to

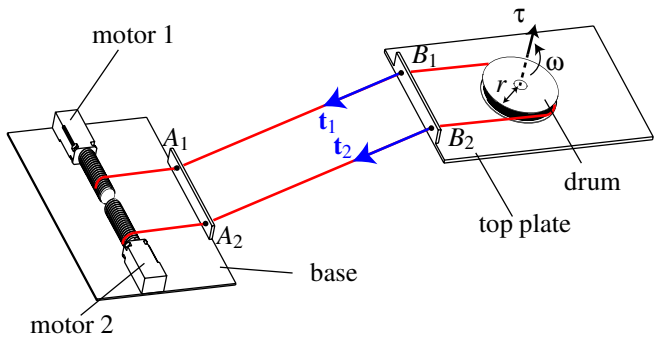

Figure 3: Representation of a cable-loop

translate the top plate as two single cables would do when the coiling directions of both motors are the same. Secondly, it actuates the embedded pulley by circulating the cable when coiling directions of the two actuators are different.

By controlling the difference of tension in both ends of the cable loop, namely $\delta t_{12} = t_1 - t_2$, it is possible to transmit torque τ to the pulley. This capacity can be used to increase the orientation workspace of the end-effector when the pulley is used to rotate the end-effector or the pulley can actuate an embedded mechanism without having the drawbacks of embedding the actuators on the platform. Here, three cable loops are used to actuate independently the three omni-wheels in contact with the sphere as illustrated in Fig. 3.

2.4 OVERALL PARAMETERIZATION

As shown in Fig. 1, $\mathcal{F}_0$ denotes the frame fixed to the base of origin point O_0 and axes x_0, y_0 and z_0. $\mathcal{F}_1$ is the frame attached to the top-plate of origin point O_1 and axes x_1, y_1 and z_1. $\mathcal{F}_2$ is the frame attached to the end-effector, i.e., the sphere, of origin point O_2, the geometric center of the sphere and axes x_2, y_2 and z_2.

It is noteworthy that $\mathcal{F}_0$ and $\mathcal{F}_1$ have a translational and orientational relative movement while $\mathcal{F}_1$ and $\mathcal{F}_2$ only have a relative rotational movement.

The exit points A_i are the points belonging to the frame through which the cables are routed between the winch and the top plate. The anchor points B_i are the points belonging to the TP where the cables are connected. It is noteworthy that the cables are connecting exit point and anchor points accordingly and a unit vector expresses the cable direction. Therefore, the loop-closure equations associated with each cable are expressed as follows:

$$ {}^0\mathbf{l}_i = {}^0\mathbf{a}_i - {}^0\mathbf{p} - {}^0\mathbf{R}_1\,{}^1\mathbf{b}_i \tag{1} $$

with $i \in [\![1,\ldots,8]\!]$ where ${}^0\mathbf{l}_i$ is the i-th cable vector, ${}^0\mathbf{a}_i$ is the

corresponding anchor point expressed in the base frame, ${}^1\mathbf{b}_i$ is the coordinate vector of exit point in the platform frame, ${}^0\mathbf{p}$ is the position vector of the platform frame and ${}^0\mathbf{R}_1$ is the rotation matrix from $\mathcal{F}_0$ to $\mathcal{F}_1$.

We can then write the i-th unit cable vector as:

$$ {}^0\mathbf{u}_i = \frac{{}^0\mathbf{l}_i}{l_i} \tag{2} $$

with l_i being the i-th cable length.

3 KINETOSTATIC MODEL OF THE MANIPULATOR

In this section, we proceed to the kinetostatic modelling of the overall manipulator. We write the static equation of the manipulator as follows:

$$ \mathbf{W}\mathbf{t} + \mathbf{w}_e = \mathbf{0}_9 \tag{3} $$

with $\mathbf{W}$ being the wrench matrix, $\mathbf{t}$ being the cable tension vector and $\mathbf{w}_e$ being the external wrenches applied on the platform. In our case, we only consider the action of the weight of the moving platform as external wrench.

The wrench matrix of the manipulator $\mathbf{W}$ is the concatenation of the wrench matrices of both mechanisms:

$$ \mathbf{W} = \begin{bmatrix} \mathbf{W}_{TP} \\ \mathbf{W}_{SW} \end{bmatrix}_{9\times 8} \tag{4} $$

where $\mathbf{W}_{TP}$ is the wrench matrix associated to the top plate and $\mathbf{W}_{SW}$ is the wrench matrix related to the PSW.

Similarly, the wrench vector of the manipulator consists of the wrench vector of both mechanisms:

$$ \mathbf{w}_g = \begin{bmatrix} \mathbf{w}_g^{TP} \\ \mathbf{w}_g^{SW} \end{bmatrix}_{9\times 1} \tag{5} $$

where $\mathbf{w}_g^{TP}$ is the wrench vector associated to the top plate and $\mathbf{w}_g^{SW}$ is the wrench vector exerted on the PSW. $\mathbf{W}_{TP}$ and $\mathbf{w}_g^{TP}$ are defined in Section 3.1 while $\mathbf{W}_{SW}$ and $\mathbf{w}_g^{SW}$ are defined in Section 3.2.

3.1 KINETOSTATIC MODEL OF THE TOP PLATE

In this section we write the kinetostatic model of the top plate. The static equilibrium of the platform can be written as:

$$ \mathbf{W}_{TP}\mathbf{t} + \mathbf{w}_g^{TP} = \mathbf{0}_8 \tag{6} $$

$\mathbf{W}_{TP}$ takes the following form:

$$ \mathbf{W}_{TP} = \begin{bmatrix} \mathbf{u}_1 & {}^0\mathbf{u}_2 & {}^0\mathbf{u}_3 & {}^0\mathbf{u}_4 & {}^0\mathbf{u}_5 & {}^0\mathbf{u}_6 & {}^0\mathbf{u}_7 & {}^0\mathbf{u}_8 \\ {}^0\mathbf{d}_1 & {}^0\mathbf{d}_2 & {}^0\mathbf{d}_3 & {}^0\mathbf{d}_4 & {}^0\mathbf{d}_5 & {}^0\mathbf{d}_6 & {}^0\mathbf{d}_7 & {}^0\mathbf{d}_8 \end{bmatrix}_{6\times 8} \tag{7} $$

with ${}^0\mathbf{d}_i$ being the cross-product matrix of vector $\mathbf{b}_i$ and $\mathbf{u}_i$

$$ {}^0\mathbf{d}_i = {}^0\mathbf{R}_1\,{}^1\mathbf{b}_i \times {}^0\mathbf{u}_i \tag{8} $$

We define the wrench vector of the top plate $\mathbf{w}_{TP}$ as follows:

$$ \mathbf{w}_g^{TP} = \begin{bmatrix} \mathbf{f}_{TP} \\ \mathbf{m}_{TP} \end{bmatrix}_{6\times 1} \tag{9} $$

where $\mathbf{f}_{TP}$ is the 3-dimensional force and $\mathbf{m}_{TP}$ is the 3-dimensional moment exerted on the top plate.

3.2 KINETOSTATIC MODEL OF THE PARALLEL SPHERICAL WRIST

The parametrization of the parallel spherical wrist is shown in Figure 4 and expressed as follows:

- C_i : Contact point between the omni-wheel and the sphere
- π_i : Plane passing through the contact point C_i and tangent to the sphere
- μ_i : Unit tangent vector of i-th omni-wheel along line t
- α : Angle associated to the position of the contact points C_i ($\alpha \in [0,\pi]$), on the sphere
- β : Angle between tangent to the sphere and the actuation force of the omni-wheel ($\beta \in [-\frac{\pi}{2},\frac{\pi}{2}]$)
- γ_2 : Angle between the contact points C_1 and C_2
- γ_3 : Angle between the contact points C_1 and C_3
- r_s : Radius of the sphere
- r_o : Radius of the omni-wheels
- $\dot{\varphi}_i$: Angular velocity of the i-th omni-wheel
- f_{ni} : Actuation force produced by the i-th omni-wheel on the sphere

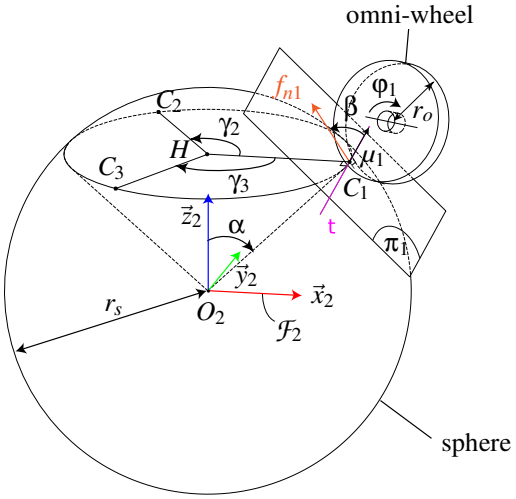

Figure 4: Parametrization of the Parallel Spherical Wrist

The optimal set of the parameters of the wrist was defined in [14] in order to maximize the amplitudes of its orientation as well its dexterity. The following hypotheses are taken into account for the further analysis and modelling:

1. The omni-wheels are normal to the sphere.
2. The contact points between the omni-wheels and the sphere belong to the circumference of a circle. The latter is the base of an inverted cone, its tip being the centre of the sphere. The angle between the vertical axis and the cone is named α.
3. In the plane containing the cone base, the three contact points form an equilateral triangle.

By taking into account the hypotheses, α and β are calculated as follows [14]:

$$\begin{aligned} \alpha &= 35.2^\circ \\ \beta &= 0^\circ \end{aligned} \tag{10}$$

The angular velocity vector of the sphere $\omega = [\omega_x, \omega_y, \omega_z]^T$ is expressed as a function of the angular velocity vector of the omni-wheels $\dot{\varphi} = [\dot{\varphi}_1, \dot{\varphi}_2, \dot{\varphi}_3]^T$, as follows:

$$\mathbf{A}\omega = \mathbf{B}\dot{\varphi} \tag{11}$$

$\mathbf{A}$ and $\mathbf{B}$ are the forward and inverse Jacobian matrices of the PSW, which take the form:

$$\mathbf{A} = \frac{r_s}{2}\begin{bmatrix} -2C_\alpha C_\beta & -2S_\beta & 2S_\alpha C_\beta \\ C_\alpha C_\beta + \sqrt{3}S_\beta & S_\beta - \sqrt{3}C_\alpha C_\beta & 2S_\alpha C_\beta \\ C_\alpha C_\beta - \sqrt{3}S_\beta & S_\beta + \sqrt{3}C_\alpha C_\beta & 2S_\alpha C_\beta \end{bmatrix} \tag{12}$$

and,

$$\mathbf{B} = r_o \mathbf{1}_{3\times 3} \tag{13}$$

where, r_s is the sphere radius, r_o is the omni-wheel radius, $S_i = \sin(i)$ and $C_i = \cos(i)$, $i = \alpha, \beta$. Notice that the radii of the omni-wheels are identical. Equation (11) is then rewritten as follows:

$$\omega = \mathbf{J}_\omega \dot{\varphi} \tag{14}$$

where $\mathbf{J}_\omega = \mathbf{A}^{-1}\mathbf{B}$, is the Jacobian matrix of the wrist, i.e., $\mathbf{J}_\omega$ is the mapping from angular velocities of the omni-wheels into the required angular velocity of the end-effector. Based on the theory of reciprocal screws [15], it turns out that:

$$\mathbf{m}_{SW}^T \omega = \tau^T \dot{\varphi} \tag{15}$$

where $\mathbf{m}_{SW} = [m_x, m_y, m_z]^T$ is the output moment vector of the sphere and $\tau = [\tau_1, \tau_2, \tau_3]^T$ is the input torque vector, namely the omni-wheel torque vector. By substituting Eq. (14) into Eq. (15), we obtain:

$$\tau = \mathbf{J}_\omega^T \mathbf{m}_{SW} = \mathbf{W}_\omega \mathbf{m}_{SW} \tag{16}$$

The wrench matrix $\mathbf{W}_\omega = \mathbf{J}_\omega^T$ maps the output torque of the sphere to the omni-wheels torques. As shown in Figure 5, it is possible to express τ as a function of cable tensions so that:

$$\tau_1 = r_o(t_1 - t_2) \tag{17}$$
$$\tau_2 = r_o(t_3 - t_4) \tag{18}$$
$$\tau_3 = r_o(t_5 - t_6) \tag{19}$$

From Equations (17) to (19), the omni-wheel torque vector τ is expressed as a function of the the cable tension vector as follows:

$$\tau = \mathbf{W}_c \mathbf{t} \tag{20}$$

where:

$$\mathbf{W}_c = \begin{bmatrix} r_o & -r_o & 0 & 0 & 0 & 0 & 0 & 0 \\ 0 & 0 & r_o & -r_o & 0 & 0 & 0 & 0 \\ 0 & 0 & 0 & 0 & r_o & -r_o & 0 & 0 \end{bmatrix} \tag{21}$$

and $\mathbf{t} = [t_1, \ldots, t_8]^T$ is the cable tension vector.

The equilibrium of the wrench applied on the PSW is written in the following:

$$\mathbf{m}_{\mathrm{SW}} = \mathbf{W}_{\mathrm{SW}} \mathbf{t} \tag{22}$$

with $\mathbf{m}_{\mathrm{SW}}$ being the external moments applied by the environment onto the PSW. The wrench matrix expresses the relation between cable tensions and the wrist moments as:

$$\mathbf{W}_{\mathrm{SW}} = \mathbf{W}_{\omega} \mathbf{W}_{\mathrm{c}} \tag{23}$$

In Figure 6, the orientation of the sphere with respect to the base frame is parametrized with angles pitch, θ, yaw, ψ, and roll, χ angles. Those three angles are the components of the orientation vector $\mathbf{q}_{SW}$ of the wrist, namely,

$$\mathbf{q}_{SW} = \begin{bmatrix} \theta \\ \psi \\ \chi \end{bmatrix} \tag{24}$$

4 WORKSPACE ANALYSIS

The static workspace of the manipulator consists of the set of positions and orientations of the moving platform and the orientations of the end-effector, namely, ${}^0\mathbf{p}$ and ${}^0\mathbf{R}_{TP}$ and ${}^0\mathbf{q}_{SW}$, which satisfies the static equilibrium of the manipulator.

The cable tension set $\mathcal{T}$ amounts to a hyper-cube in an eight-dimensional space:

$$\mathcal{T} = \{\mathbf{t} \in \mathbb{R}^8 : \mathbf{t}_{min} \leq \mathbf{t} \leq \mathbf{t}_{max}\} \tag{25}$$

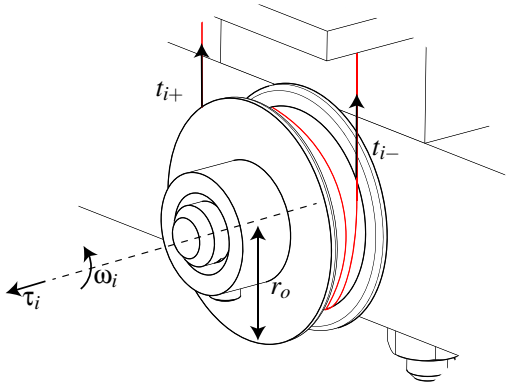

Figure 5: Representation of a cable-loop drum

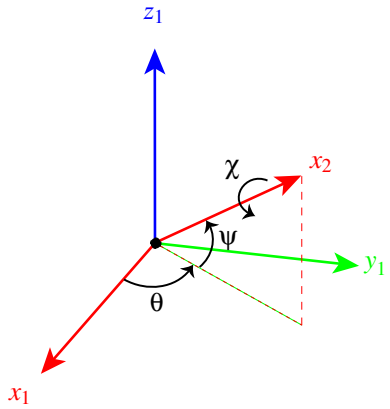

Figure 6: Rotation angles of the wrist

where $\mathbf{t}_{min}$ and $\mathbf{t}_{max}$ are respectively the lower and upper bounds of the cable tension.

The static workspace of the manipulator is defined as follows:

$$\mathcal{S} = \{({}^0\mathbf{p}, {}^0\mathbf{R}_{TP}, {}^0\mathbf{q}_{SW} \in \mathbb{R}^3 \times SO(3) \times \mathbb{R}^3 : \exists \mathbf{t} \in \mathcal{T}, \mathbf{W}\mathbf{t} + \mathbf{w}_e = \mathbf{0}_9\} \tag{26}$$

where $SO(3)$ is the group of proper rotation matrices. The static workspace in a nine-dimensional space is expressed using the Equation (26). As the visualization of such high-dimensional space is impossible with common human perception in 3D, we define the static workspace of the manipulator for a simplified case. We define $\mathcal{S}$ for a constant orientation of the top-plate. The former subset, namely, $\mathcal{S}_{AO}$ is a set for a given orientation of the top-plate while the wrist is free to rotate:

$$\mathcal{S}_{AO} = \{{}^0\mathbf{p} \in \mathbb{R}^3 \,|\, {}^0\mathbf{R}_1 = \mathbf{I}_3 | -\pi \leq \theta,\ \psi,\ \chi \leq \pi : \exists \mathbf{t} \in \mathcal{T},\ \mathbf{W}\mathbf{t} + \mathbf{w}_e = \mathbf{0}_9\} \quad (27)$$

The discretization of the Cartesian space is made so that n_x, n_y and n_z are the numbers of discretized points along $\vec{x}_0$, $\vec{y}_0$ and $\vec{z}_0$ axes, respectively.

$\mathcal{R}_\mathcal{S}$ is defined as the proportion of the static workspace to the overall space occupied by the manipulator:

$$\mathcal{R}_\mathcal{S} = \frac{N_\mathcal{S}}{(n_x+1)(n_y+1)(n_z+1)} \quad (28)$$

with $N_\mathcal{S}$ being the number of points inside the discretized static workspace $\mathcal{S}$.

5 OPTIMAL CABLE ARRANGEMENT

This section deals with the cable arrangement of the manipulator for obtaining the maximum size of the static workspace. The $i-$th cable arrangement is the association of anchor points B_i to exit points A_i. The top plate has fifteen points for anchor points and the manipulator has a maximum of eight actuators. Therefore, the optimal cable arrangement is defined as the association of eight anchor points to eight exit points such that the workspace is maximized.

The number of exit point combinations, $\mathcal{N}_e$ is:

$$\mathcal{N}_e = \binom{n_e}{n_c} \quad (29)$$

with n_e and n_c being the numbers of available exit-points and cables, respectively. The number of anchor-points combinations, $\mathcal{N}_a$, consists in the number of permutations of the set of points, which is given by:

$$\mathcal{N}_a = \binom{n_a}{n_c} n_c! \quad (30)$$

n_a being the number of selected anchor-points. $\mathcal{S}_C$ is the set of possible cable configuration, the number of configuration $\mathcal{N}_C = dim(\mathcal{S}_C)$ is thus given by:

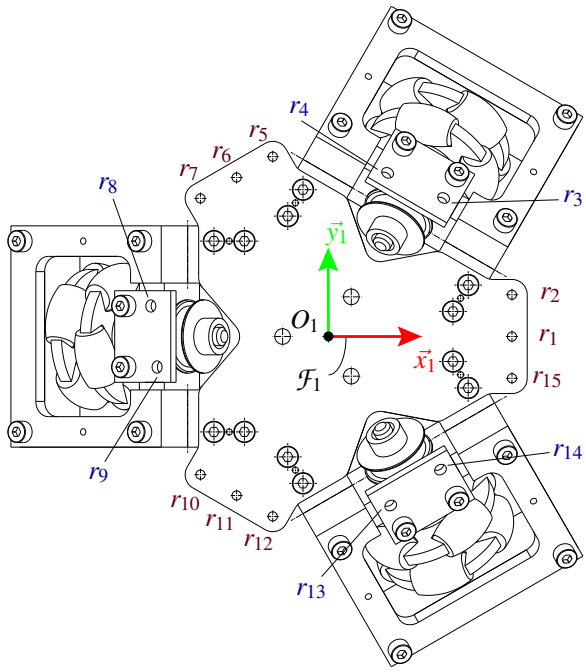

Figure 7: The fifteen points for the anchor points on the moving-platform

$$\mathcal{N}_c = \mathcal{N}_a \mathcal{N}_e = \binom{n_e}{n_c} \binom{n_a}{n_c} n_c! \quad (31)$$

Figure 7 shows all the available anchor points, namely, r_i, $i = 1,\ 2,\ \ldots,\ 15$, which are divided into two groups: $\mathcal{S}_{\text{CL}} = \{r_3, r_4, r_8, r_9, r_{13}, r_{14}\}$ which is the set of points associated to cable-loops and $\mathcal{S}_{\text{SC}} = \{r_1, r_2, r_5, r_6, r_7, r_{10}, r_{11}, r_{12}, r_{15}\}$ which is the set of points associated to the simple cables. Six points amongst the fifteen points are selected to make the three cable loops. Therefore, nine remaining anchor points host the remaining two single-actuated cables.

$$n_c = n_{SC} + n_{CL} \quad (32)$$

The number of available anchor points for the single and bi-actuated cables are denoted as n_{aSC} and n_{aCL}:

$$n_a = n_{aSC} + n_{aCL} \quad (33)$$

The number, $\mathcal{N}_{CL}$, of combinations considering cable-loop is given by:

$$\mathcal{N}_{CL} = \binom{n_e}{n_c}\binom{n_{aSC}}{n_{SC}} n_c! \tag{34}$$

Six points are associated to the wrist actuation and consequently to the three cable-loops: $n_{aCL} = 6$. The remaining nine anchor points are to be assigned to simple cables $n_{aSC} = 9$. Finally, $\mathcal{N}_{CL}$, expressed in Eq. (34) is given by:

$$\mathcal{N}_{CL} = \binom{8}{8}\binom{9}{2} 8! = 1\,451\,520 \tag{35}$$

As $\mathcal{N}_{CL}$ is very large, for computing-time sake, the number of available points for anchor points is supposed to be equal to three. Thus $\mathcal{S}_{SC} = \{r_1, r_6, r_{11}\}$. By substituting $n_{aSC} = 3$ into Eq. (34) we obtain:

$$\mathcal{N}_{CL} = \binom{8}{8}\binom{3}{2} 8! = 120\,960 \tag{36}$$

The static workspace is computed for the 120 960 cable arrangements. Figure 8 illustrates the cable arrangement corresponding to the largest workspace. Figure 8a shows a schematic of the anchor-plate as well as the optimal cable arrangement. Figure 8b shows the corresponding static workspace with $\mathcal{R}_S = 65\%$.

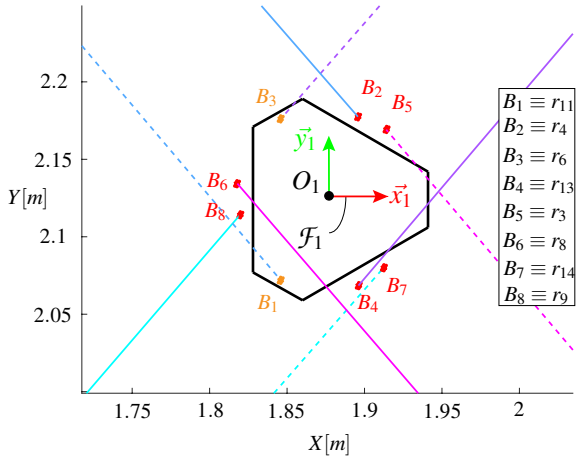

(a) Cable configuration

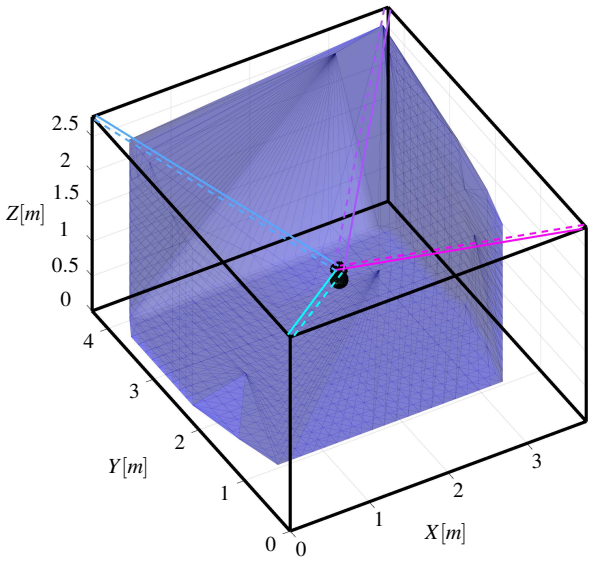

(b) Static workspace

Figure 8: Results of the optimization algorithm

6 EXPERIMENTAL DEMONSTRATOR

An experimental demonstrator of the manipulator was manufactured as shown in Figure 9. The architecture of the manipulator with an embedded PSW is presented in Figure 10. The main hardware of the CREATOR demonstrator consists of a PC (equipped with ©MATLAB and ©ControlDesk software), ©PARKER SME60 motors and TPD-M drivers, a ©dSPACE DS1007-based real-time controller and custom made winches.

The experimental setup allows us to evaluate the capabilities of the manipulator in operation. However, there is one crucial constraint imposed by the demonstrator setup in terms of number of actuators. Since the manipulator has nine-DOFs and the demonstrator is equipped with only eight motors, the overall system is underactuated. Her the performance of the manipulator is assessed by considering the following cases:

Case 1: The moving platform is over-actuated with six controllable DOFs of the top-plate. Hence, the desired trajectory includes the translational motion of the top-plate within the workspace while fixing the orientation of the top-plate as well as the PSW. This link [1] refers to a video of this case.

Case 2: The pose of the top-plate is mechanically constrained and the orientation of the wrist is controlled. This case aims to illustrate the performance of the PSW regardless of the parasitic inclinations due to under-actuation. This video link [2] illustrates this case.

Case 3: The control of 8-DOFs of the manipulator, i.e., leaving free the rotation of the top-plate about the vertical axis, namely, z_0. As a consequence, parasitic inclinations arise. This case shows the under-actuation effects imposed onto

[1] https://metillon.net/3T3R_1
[2] https://metillon.net/3T3R_2

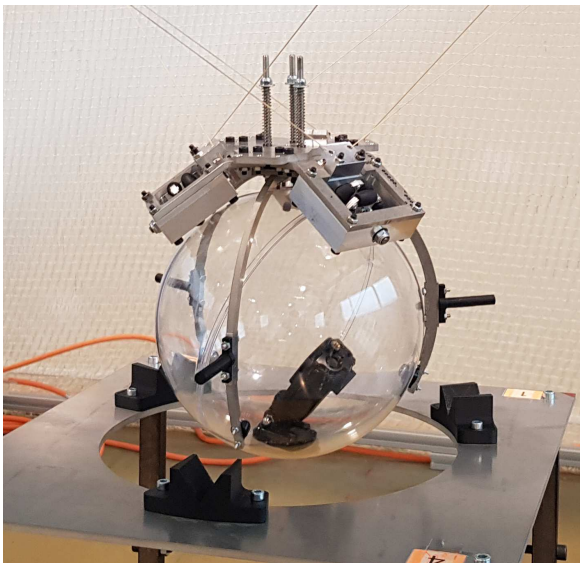

Figure 9: The moving platform with full-circle end-effector

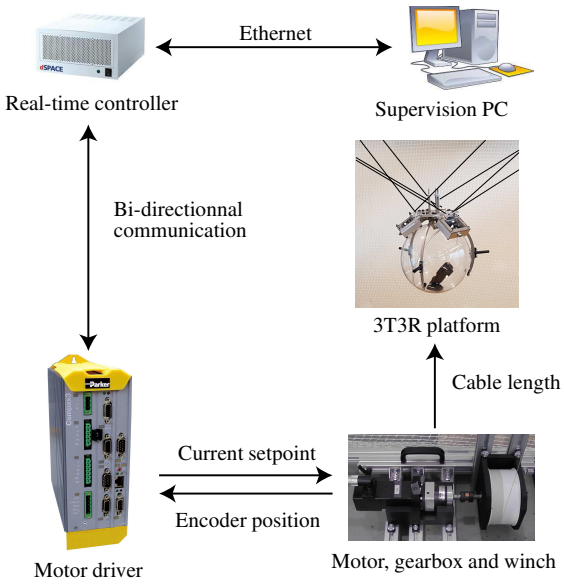

Figure 10: Control architecture of the manipulator

the system due to an insufficient number of actuators. A video illustrating this case is given link [3].

7 CONCLUSIONS AND FUTURE WORK

This paper addressed the novel design of a cable driven parallel robot with an embedded parallel spherical wrist. The mechanism has nine degrees of freedom. A complete kinetostatic model of the overall moving platform was expressed. The cable arrangement was optimized in order to maximise the static workspace. Moreover a set of preliminary experiments illustrates the capabilities of the mechanism in term of translation and orientation.

The overall system is underactuated because the moving-platform has nine degree of freedom and eight actuators only are used. Later on, the parasitic inclinations of the end-effector will be studied in order to find some strategies to compensate them.

[3] https://metillon.net/3T3R_3

ACKNOWLEDGMENT

This work was supported by both the ANR CRAFT project, grant ANR-18-CE10-0004 and the RFI AtlanSTIC2020 CREATOR project.

REFERENCES

[1] Hussein, H., Santos, J. C., and Gouttefarde, M., 2018. "Geometric optimization of a large scale cdpr operating on a building facade". In 2018 IEEE/RSJ International Conference on Intelligent Robots and Systems (IROS), IEEE, pp. 5117–5124. 1

[2] Kawamura, S., Choe, W., Tanaka, S., and Pandian, S. R., 1995. "Development of an ultrahigh speed robot falcon using wire drive system". In Proceedings of 1995 IEEE International Conference on Robotics and Automation, IEEE, pp. 215–220. 1

[3] Gagliardini, L., Caro, S., Gouttefarde, M., and Girin, A., 2016. "Discrete reconfiguration planning for cable-driven parallel robots". *Mechanism and Machine Theory,* ***100***, pp. 313–337. 1

[4] Pedemonte, N., Rasheed, T., Marquez-Gamez, D., Long, P., Hocquard, E., Babin, F., Fouch, C., Caverot, G., Girin, A., and Caro, S., 2020. *FASTKIT: A Mobile Cable-Driven Parallel Robot for Logistics*, springer, cham ed., Vol. 132. pp. 141–163. 1

[5] Rasheed, T., Long, P., and Caro, S., 2020. "Wrench-feasible workspace of mobile cable-driven parallel robots". *Journal of Mechanisms and Robotics, American Society of Mechanical Engineers,* ***12***(3), p. 031009. 1

[6] Qian, S., Zi, B., Shang, W.-W., and Xu, Q.-S., 2018. "A review on cable-driven parallel robots". p. 1007. PII: 267. 1

[7] Bak, J.-H., Hwang, S. W., Yoon, J., Park, J. H., and Park, J.-O., 2019. "Collision-free path planning of cable-driven parallel robots in cluttered environments". pp. 243–253. PII: 278. 1

[8] Merlet, J.-P., 2006. *Parallel robots*, 2nd ed. ed., Vol. 74 of *Solid mechanics and its applications*. Kluwer Academic Publishers. 2

[9] Vikranth Reddy, M., Praneet, N. C., and Ananthasuresh, G. K., 2019. "Planar cable-driven robots with enhanced orientability". In *Cable-Driven Parallel Robots*, A. Pott and T. Bruckmann, eds., Vol. 74 of *Mechanisms and Machine Science*. Springer International Publishing, pp. 3–12. 2

[10] Lessanibahri, S., Cardou, P., and Caro, S., 2018. "Kinetostatic analysis of a simple cable-driven parallel crane". In Volume 5A: 42nd Mechanisms and Robotics Conference, American Society of Mechanical Engineers. 2

[11] Lessanibahri, S., Cardou, P., and Caro, S., 2019. "A cable-driven parallel robot with an embedded tilt-roll wrist". In Volume 5A: 43rd Mechanisms and Robotics Conference, American Society of Mechanical Engineers. 2

[12] Lessanibahri, S., Cardou, P., and Caro, S., 2020. "A cable-driven parallel robot with an embedded tilt-roll wrist". *Journal of Mechanisms and Robotics, American Society of Mechanical Engineers,* ***12***(2), pp. 021107–1 021107–10. 2

[13] Hayes, M., and Langlois, R. G., 2005. "Atlas: A novel kinematic architecture for six dof motion platforms". pp. 701–709. 2

[14] Platis, A., Rasheed, T., Cardou, P., and Caro, S., 2017. "Isotropic design of the spherical wrist of a cable-driven parallel robot". In *Advances in robot kinematics*, J. Lenarčič and J.-P. Merlet, eds., Vol. 4 of *Springer Proceedings in Advanced Robotics*. Springer Berlin Heidelberg, pp. 321–330. 3, 5

[15] Ball, R. S., 1900. *A treatise on the theory of screws, by Sir Robert Stawell Ball*. University Press. 5